The Crystal Structure of *Mycobacterium tuberculosis* Thymidylate Kinase in Complex with 3′-Azidodeoxythymidine Monophosphate Suggests a Mechanism for Competitive Inhibition[†,‡]

Emanuela Fioravanti,[§,||] Virgile Adam,[§,||] Hélène Munier-Lehmann,[⊥] and Dominique Bourgeois*[,§,||]

LCCP, UMR 5075, IBS-CEA/CNRS/UJF, 41 avenue Jules Horowitz, 38027 Grenoble Cedex 1, France, ESRF, 6 rue Jules Horowitz, BP 220, 38043 Grenoble Cedex, France, and Unité de Chimie Organique, URA CNRS 2128, Institut Pasteur, 28 rue du Docteur Roux, 75724 Paris Cedex 15, France

Received July 26, 2004; Revised Manuscript Received October 26, 2004

ABSTRACT: Tuberculosis (TB) is the primary cause of mortality among infectious diseases. *Mycobacterium tuberculosis* thymidylate kinase ($TMPK_{Mtub}$) catalyzes the ATP-dependent phosphorylation of deoxythymidine 5′-monophosphate (dTMP). Essential to DNA replication, this enzyme represents a promising target for developing new drugs against TB, because the configuration of its active site is unique within the TMPK family. Indeed, it has been proposed that, as opposed to other TMPKs, catalysis by $TMPK_{Mtub}$ necessitates the transient binding of a magnesium ion coordinating the phosphate acceptor. Moreover, 3′-azidodeoxythymidine monophosphate (AZTMP) is a competitive inhibitor of $TMPK_{Mtub}$, whereas it is a substrate for human and other TMPKs. Here, the crystal structures of $TMPK_{Mtub}$ in complex with deoxythymidine (dT) and AZTMP were determined to 2.1 and 2.0 Å resolution, respectively, and suggest a mechanism for inhibition. The azido group of AZTMP perturbs the induced-fit mechanism normally adopted by the enzyme. Magnesium is prevented from binding, and the resulting electrostatic environment precludes phosphoryl transfer from occurring. Our data provide a model for drug development against tuberculosis.

Tuberculosis is a major disease of mankind, claiming more than 2 million lives annually (*1*). One of the most significant risk factors for developing TB is infection by the human immunodeficiency acquired virus (HIV).[1] Moreover, TB is the most likely cause of death for HIV-positive people. Because of the appearance of multiresistant strains (*2*) and the lack of an effective vaccine, the quest for new drugs against TB has become a priority.

Thymidylate kinase (TMPK, EC 2.7.4.9, ATP:TMP phosphotransferase) belongs to the nucleoside monophosphate kinase (NMPK) family and catalyzes the reversible phosphorylation of dTMP to deoxythymidine 5′-diphosphate (dTDP) in the presence of adenosine triphosphate (ATP). Situated at the junction of the *de novo* and salvage pathways for the synthesis of deoxythymidine 5′-triphosphate (dTTP), TMPK is the last specific enzyme in these pathways, therefore being essential for cell growth and survival. TMPKs are homodimers, each monomer being composed of eight to nine α-helices surrounding a five-stranded *β*-sheet core. Two essential structural features of all TMPKs are a phosphate binding loop (P-loop) at the N-terminus that includes a strictly conserved aspartate (or glutamate) residue and the LID region, a highly flexible stretch of residues covering the phosphate donor binding site at the C-terminus (*3*, *4*).

The enzyme from *Mycobacterium tuberculosis* is a particularly valuable target for the development of new therapies against TB because it uses a catalytic mechanism unique within the TMPK family. Indeed, a combined analysis of several X-ray structures of the enzyme indicates that, as opposed to other known TMPKs, phosphate transfer in $TMPK_{Mtub}$ requires the transient binding of a magnesium ion coordinating the phosphate acceptor (*5*−*8*). For example, it was shown that the presence of a metal ion in the dTMP binding site correlates with the observation of a catalytic activity of the crystalline enzyme (*6*, *7*). Magnesium compensates for a missing positively charged residue (Arg45 in the human enzyme is replaced with Tyr39 in $TMPK_{Mtub}$) and plays a key role in neutralizing the electrostatic repulsion between the anionic substrates. The 3′-hydroxyl (3′-OH)

[†] This work was supported by grants from the Institut Pasteur, the Institut National de la Santé et de la Recherche Médicale, and the Centre National de la Recherche Scientifique. E.F. was supported by an ESRF Ph.D. fellowship.

[‡] Coordinates and structure factor amplitudes of the $TMPK_{Mtub}$−dT and $TMPK_{Mtub}$−AZTMP structures have been deposited in the RSCB Protein Data Bank as entries 1W2G and 1W2H, respectively.

* To whom correspondence should be addressed: LCCP, UMR 5075, IBS-CEA/CNRS/UJF, 41 avenue Jules Horowitz, 38027 Grenoble Cedex 1, France. Telephone: (33) (0) 4 38 78 96 44. Fax: (33) (0) 4 38 78 51 22. E-mail: dominique.bourgeois@ibs.fr.

[§] IBS-CEA/CNRS/UJF.

[||] ESRF.

[⊥] URA CNRS 2128.

[1] Abbreviations: TB, tuberculosis; NMPK, nucleoside monophosphate kinase; TMPK, thymidylate kinase; $TMPK_{Mtub}$, *M. tuberculosis* thymidylate kinase; dT, deoxythymidine; dTMP, deoxythymidine 5′-monophosphate; dTDP, deoxythymidine 5′-diphosphate; dTTP, deoxythymidine 5′-triphosphate; AZTMP, 3′-azidodeoxythymidine monophosphate; ATP, adenosine triphosphate; HIV, human immunodeficiency virus; P-loop, phosphate binding loop; rmsd, root-mean-square deviation.

10.1021/bi0484163 CCC: $30.25
Published on Web 12/13/2004

group of dTMP, adopting a C2′-endo conformation in the active site, participates in metal stabilization through interactions involving a central water molecule (Wat141) and Asp9, the conserved acidic residue of the P-loop. Hence, this group has been highlighted as a target of election for the design of inhibitors against the enzyme (*6*, *8*). Solution studies have revealed that some dTMP analogues substituted at position 3′ or 2′ of the ribose moiety and/or at position 5 of the thymine ring inhibit the enzyme with K_i values in the range of 5−50 μM (*9*−*11*). In particular, AZTMP inhibits $TMPK_{Mtub}$ in a competitive manner at the phosphate acceptor site with a K_i of ∼10 μM (*9*). Interestingly, some nonphosphorylated thymidine analogues, two of which are dT and 3′-azido-3′-deoxythymidine (AZT), also inhibit the enzyme (*12*−*14*).

The case of AZTMP is particularly relevant since this molecule is a substrate for almost all TMPK enzymes studied so far (*15*−*18*). The rate of phosphorylation by the *Escherichia coli* enzyme is only 2-fold lower for AZTMP than it is for dTMP. The human enzyme participates in the activation pathway of the anti-HIV pro-drug AZT, but phosphorylates AZTMP only at a low rate, creating a bottleneck in this pathway (*19*) that contributes to the toxicity and limited efficacy of AZT therapy. The difference in the efficiency of AZTMP phosphorylation between eukaryotic and prokaryotic TMPKs has been correlated to subtle variations in the interaction of the azido moiety with the conserved aspartate or glutamate in the P-loop (*16*). The striking difference in the behavior of $TMPK_{Mtub}$ toward AZTMP compared to that of other TMPKs should now be addressed in view of the peculiar mechanism adopted by the *M. tuberculosis* enzyme.

In this work, we determined the crystal structures of $TMPK_{Mtub}$ in complex with AZTMP and dT to 2.0 and 2.1 Å resolution, respectively. The results provide structural evidence that AZTMP inhibits $TMPK_{Mtub}$ through a simple mechanism: the presence of the azido moiety prevents the binding of the Mg^{2+} ion essential to catalysis. This finding may serve as a basis for the rational design of drugs against TB. Furthermore, the structure of the $TMPK_{Mtub}$−AZTMP complex reveals that AZTMP may also bind in the ATP active site, consistent with the substrate inhibition mechanism contributing to AZT toxicity suggested for the human enzyme (*19*).

MATERIALS AND METHODS

Crystallization Conditions. $TMPK_{Mtub}$ was overexpressed, purified (*9*), and cocrystallized with dT and magnesium acetate, using sodium malonate as a precipitant (*6*). Cocrystallization trials with dT using ammonium sulfate as a precipitant, which normally yields crystals with higher diffraction power, failed, which we attribute to the fact that ammonium sulfate forces crystallization in an intermediate-like state of the enzyme that can only form in the presence of dTMP (*6*, *8*). Crystals of the $TMPK_{Mtub}$−AZTMP complex were obtained by soaking $TMPK_{Mtub}$−dT crystals at room temperature for ∼45 min in a solution containing 14 mM AZTMP, 1.4 M sodium malonate, 2% PEG 2000, 0.1 M MES (pH 6.0), 2 mM β-mercaptoethanol, and 25 mM magnesium acetate. All crystals were flash-cooled to 100 K for data collection, after being soaked in a cryoprotectant solution (*6*).

Table 1: Data Collection, Refinement Statistics, and Quality of Structures

	$TMPK_{Mtub}$−dT complex	$TMPK_{Mtub}$−AZTMP complex
resolution (Å)	2.1	2.0
R_{sym}[b] (%)	10.8 (41.6)[a]	11.4 (41.8)[a]
completeness (%)	99.9 (100.0)	92.2 (92.2)
redundancy	5.1	4.6
$\langle I/\sigma(I)\rangle$	13.3 (3.1)	11.6 (2.3)
R_{cryst}[c] (%)	21.1	25.9
R_{free}[d] (%)	24.4	29.6
no. of unique reflections	27923	30873
no. of protein atoms	2906	2885
no. of ligand atoms	46	77
no. of solvent atoms	153	210
no. of observations/ parameters	2.2	2.4
overall *G*-factor[e]	0.35	0.30
rmsd for bonds (Å)	0.006	0.006
rmsd for angles (deg)	1.05	1.10
Sigmaa coordinate error	0.36	0.33
average *B* factor (Å^2)	31.8	28.7

[a] Highest-resolution shells (in parentheses) are 2.21−2.10 Å for the $TMPK_{Mtub}$−dT complex and 2.11−2.0 Å for the $TMPK_{Mtub}$−AZTMP complex. For both data sets, the low-resolution limit is ∼42 Å. [b] $R_{sym} = \sum|I_{obs} - \langle I\rangle|/\sum\langle I\rangle$. [c] $R_{cryst} = \sum|F_{obs} - F_{calc}|/\sum F_{obs}$. [d] R_{free} was calculated with a small fraction (5%) of randomly selected reflections. [e] The *G*-factor is the overall measure of structure quality from PROCHECK (*34*).

X-ray Data Collection and Structure Determination. Diffraction data were collected on beamline ID-14 at ESRF (Grenoble, France) and processed with Mosflm (*20*). Data collection statistics, refinement statistics, and geometry analysis are given in Table 1. Crystals belong to space group $P3_121$ with the following mean cell dimensions: 64.2, 64.2, and 195.4 Å. The asymmetric unit accommodates the functional dimer, with a solvent content of 45%. The slightly lower quality of the data set from the $TMPK_{Mtub}$−AZTMP complex was attributed to a significant anisotropy of the diffraction power throughout the reciprocal space, resulting in a less than optimal completeness and in higher crystallographic *R*-factors.

Models of $TMPK_{Mtub}$ were refined with CNS (*21*) using bulk solvent correction and a maximum likelihood target function. Rigid body refinement was followed by standard cycles of conjugate gradient minimization and manual model building using O (*22*).

The occupancy of AZTMP in the phosphate donor site (monomer A) was estimated to be ∼65%. An acetate ion was found in the ATP site with occupancies of 35% (monomer A of the $TMPK_{Mtub}$−AZTMP structure) and 100% (monomer B of the $TMPK_{Mtub}$−AZTMP structure and both monomers of the $TMPK_{Mtub}$−dT structure).

RESULTS

Crystalline $TMPK_{Mtub}$ has previously been shown to be catalytically competent if sodium malonate is used as a precipitating agent (*6*). The X-ray structure of the enzyme crystallized with this agent and in complex with its natural substrate dTMP [Protein Data Bank (PDB) entry 1N5K] is shown in Figure 1. For clarity, we recall hereafter the essential features of this structure (*6*). In the crystal, the two monomers (termed A and B) undergo a different degree of conformational flexibility, particularly in the LID region. In

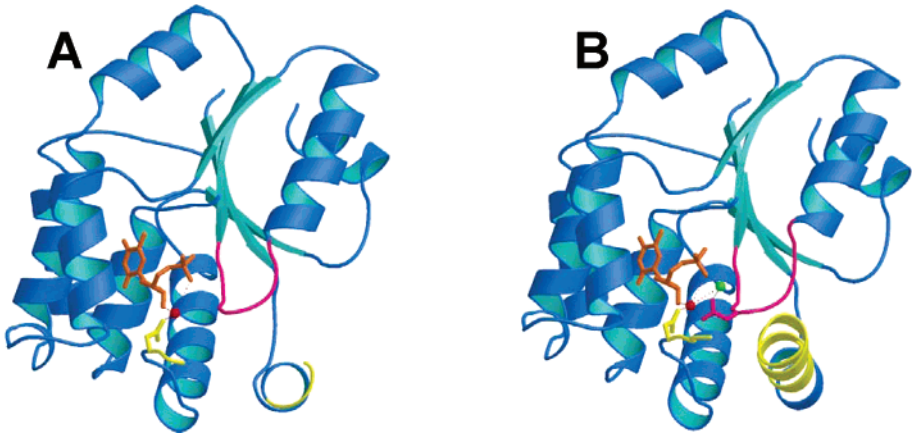

FIGURE 1: Structure of the $TMPK_{Mtub}$−dTMP complex (PDB entry 1N5K). The protein is shown in ribbon representation. The ordered part of the LID region is colored yellow and the P-loop magenta. dTMP (orange), Asp163, and Asp9 are shown in stick mode. (A) In monomer A, the active site is free of lattice contacts and no magnesium ion may bind. The dTMP substrate is sensed by interactions linking its 3′-OH group, Wat141 (red ball), and Asp163. (B) In monomer B, the active site is held in a semi-closed state by residual lattice contacts. A Mg^{2+} ion (green ball) is found in the dTMP binding site. Figures 1−6 were prepared with BOBSCRIPT (*35*) and RASTER3D (*36*).

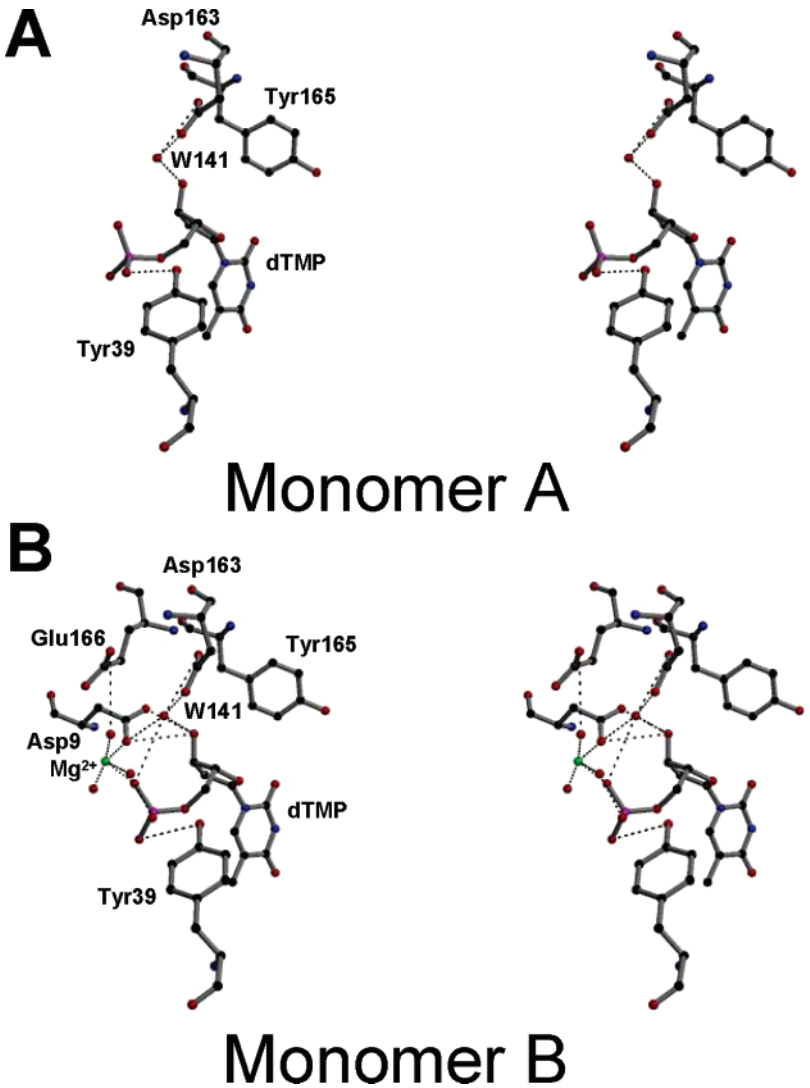

FIGURE 2: Stereoviews of the phosphate acceptor site in the $TMPK_{Mtub}$−dTMP complex: (A) monomer A and (B) monomer B. Disordered and nonessential residues are not represented. Important interactions are represented with dotted lines.

the presence of dTMP, monomer A is in a "semi-open" state with a large part of the LID being disordered. The structure of this monomer provides a picture of the first step along the reaction pathway, the binding of dTMP (Figures 1A and 2A). The substrate is "sensed" by interactions linking its 3′-OH group with Asp163, via the essential water molecule Wat141. A Mg^{2+} ion is not observed in monomer A, since at this early stage of the reaction the semi-open state of the enzyme prevents metal stabilization. In contrast, the active site of monomer B is found in a "semi-closed" state, due to

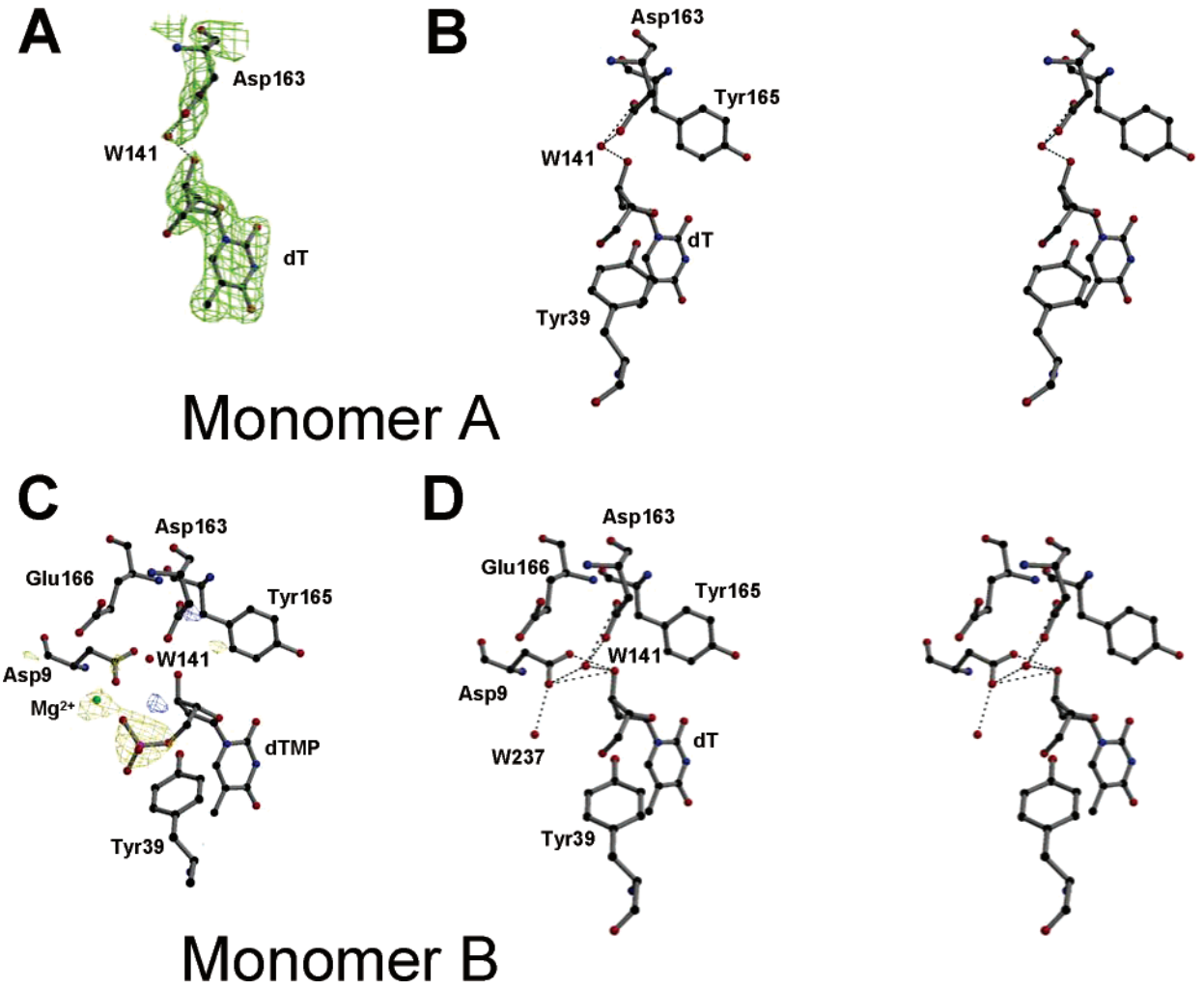

FIGURE 3: Phosphate acceptor site in the $TMPK_{Mtub}$−dT complex: (A and B) monomer A and (C and D) monomer B. Disordered and nonessential residues are not represented. Important interactions are represented with dotted lines. (A) Close view of the interactions established by the 3′-OH group of dT in monomer A. An $F_{obs} - F_{calc}$ omit electron density map, contoured at 3.0σ (in green, σ is the standard deviation of the electron density), is superimposed to the refined model. The part of the model represented on the figure has been omitted in the calculation of the (simulated annealing) omit map. (B) Stereoview of the acceptor site, monomer A. (C) Structural changes induced by the binding of dT, monomer B. The $F_{obs,dT} - F_{obs,dTMP}$ experimental difference electron density map (yellow, negative; blue, positive; contoured at $\pm 3.5\sigma$) is overlaid on the model of the $TMPK_{Mtub}$−dTMP complex (PDB entry 1N5K). This model was used for phase calculations. Negative peaks show the disappearance of Mg^{2+} (green ball) and of the α-phosphate group. (D) Stereoview of the acceptor site, monomer B.

more prominent lattice contacts. The corresponding structure has been proposed to be representative of the second step along the reaction pathway, the binding of magnesium (Figures 1B and 2B) (*6*). In this monomer, the LID is mostly organized as an α-helix, favoring the stabilization of the conserved P-loop residue Asp9 and leading to metal binding.

The structures of $TMPK_{Mtub}$ in complex with either dT or AZTMP reveal no major conformational rearrangement as compared to the structure of the $TMPK_{Mtub}$−dTMP complex (overall root-mean-square deviations from the latter structure, excluding water molecules, of 0.6 and 0.4 Å, respectively). However, subtle structural changes occur in the enzyme active site.

$TMPK_{Mtub}$−dT Complex at 2.1 Å Resolution. In this structure, in both monomers A and B, Wat141 is maintained through tight hydrogen bonds to Asp163 and to the 3′-OH group of dT, despite the absence of an α-phosphate group (Figure 3). In monomer B, the Mg^{2+} ion and two of its coordinating water molecules (Wat143 and Wat153), normally bound when dTMP is present, are no longer observed due to the loss of two contacts normally mediated by the α-phosphate group of dTMP (Figure 3C,D). In this monomer, Asp9 remains ordered and, as in the case of the $TMPK_{Mtub}$−dTMP complex, interacts with the 3′-OH group of the substrate, Tyr103, and, weakly, with Arg95 and Wat141.

$TMPK_{Mtub}$−AZTMP Complex at 2.0 Å Resolution. Crystals of the $TMPK_{Mtub}$−AZTMP complex could only be obtained in soaking experiments, by displacing dT rather than dTMP from the active site. We assign this finding to the fact that the modest difference in the affinity for the enzyme of dT ($K_i = 27\ \mu M$) and dTMP ($K_m = 4.5\ \mu M$) found in solution (*12*) is probably greatly enhanced in the crystalline state. A key advantage of this experimental protocol was that the observation in electron density maps of a phosphate group in the acceptor site proved unambiguously the occurrence of AZTMP binding even when the azido group could not be easily distinguished from the 3′-OH group of the natural substrate.

In monomer A, the azido group of AZTMP is well ordered and takes the place of Wat141, which is prevented from

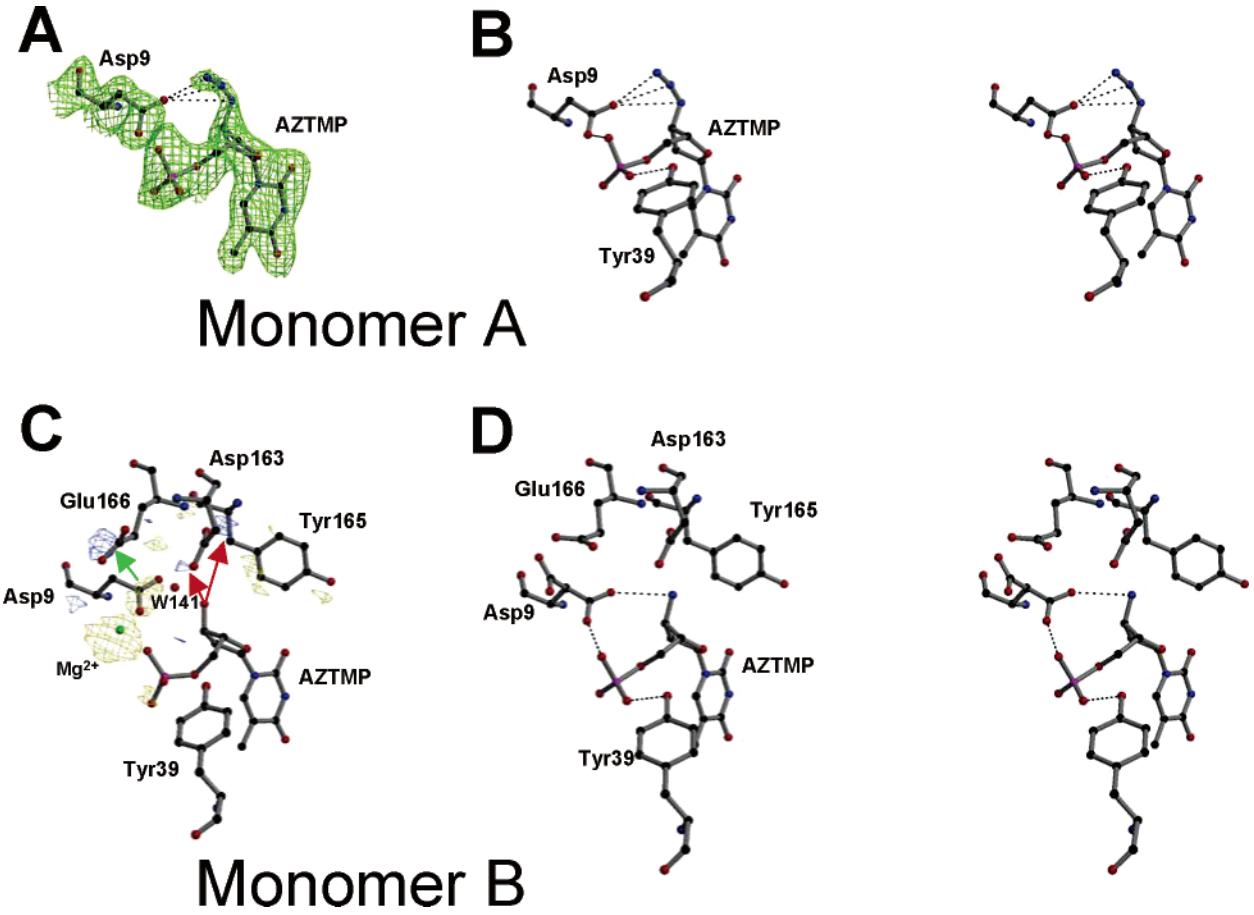

FIGURE 4: Phosphate acceptor site in the $TMPK_{Mtub}$−AZTMP complex: (A and B) monomer A and (C and D) monomer B. Disordered and nonessential residues are not represented. Important interactions are represented with dotted lines. (A) Close view of the interaction established by the 3′-azido group of AZTMP with Asp9 in monomer A. An $F_{obs} - F_{calc}$ omit electron density map, contoured at 2.5σ (green), is superimposed on the refined model. The part of the model represented on the figure has been omitted in the calculation of the (simulated annealing) omit map. In this map, a noise feature flanking the N5 atom of the azido group has been artificially suppressed for clarity. (B) Stereoview of the acceptor site, monomer A. (C) Structural changes induced by the binding of AZTMP in the acceptor site, monomer B. The $F_{obs,AZTMP} - F_{obs,dTMP}$ experimental difference electron density map (yellow, negative; blue, positive; contoured at ±3.5σ) is overlaid on the model of the $TMPK_{Mtub}$−dTMP complex. This model was used for phase calculations. Negative peaks show the disappearance of Mg^{2+} (green ball) and the destabilization of Asp9 and Tyr165. Positive peaks suggest positions for the azido moiety (red arrows) and a second conformation for Asp9 (green arrow). (D) Stereoview of the acceptor site, monomer B.

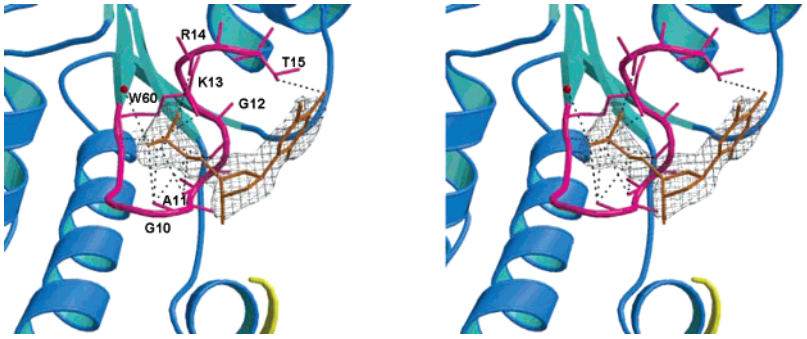

FIGURE 5: AZTMP bound to the phosphate donor site (stereoview). AZTMP is shown as orange sticks, and interactions with residues of the P-loop (magenta) and LID (yellow) are represented with dashed lines. The final $2F_{obs} - F_{calc}$ electron density map covering AZTMP at 1.0σ is shown in gray.

binding and cannot stabilize Asp163 (Figure 4A,B). The "anchoring" of Asp163 on dTMP, proposed to be the first step on the reaction pathway, promoting LID closure and Mg^{2+} binding, is therefore not possible in the presence of AZTMP. Disordering of Tyr165, normally covering the ribose moiety of the substrate, follows the destabilization of Asp163. In addition, the azido group establishes direct interactions with Asp9 (Figure 4A,B). This residue, whose side chain normally remains disordered until LID closure, is therefore prematurely and inadequately positioned so that it also interacts directly with the α-phosphate group.

Interestingly, in monomer A, a second AZTMP molecule is observed in the phosphoryl donor binding site (Figure 5), probably favored by the large accessibility of this site when the LID is open. Although the azido group is mostly disordered and could not be modeled, the base and ribose moieties are clearly identified in the electron density and interact with the protein through van der Waals contacts and

one hydrogen bond between the side chain of Thr15 and the O4 atom of the base. The α-phosphate group is found at a position putatively occupied by the *β*-phosphate of ATP (*5*), interacting with the P-loop main chain, the side chain of Lys13, and a water molecule. Nevertheless, the overall geometry of the ATP binding site is not significantly altered, and no change in the positioning of the P-loop can be noticed at the resolution of our data.

In monomer B, neither Wat141 nor a magnesium ion is observed in the presence of AZTMP (Figure 4C,D). Asp163, Tyr165, and Glu166 are observed at the same positions as in the $TMPK_{Mtub}$−dTMP complex but display higher *B*-factors. These residues are brought into position, but only loosely, by partial LID closure imposed by lattice contacts. Only the N3 atom of the azido group could be modeled in this monomer, suggesting several conformations of this group that might be induced by the nearby, conflicting presence of Asp163 and Tyr165. A swing of Asp9 to a second, partially occupied conformation corroborates this finding (Figure 4C,D). This second conformation is stabilized by hydrogen bonds to Ser150 and to a water molecule.

DISCUSSION

Chemotherapy of virus infection is often based on derivatives of natural nucleosides (*23*), which, once triphosphorylated by intracellular kinases, target viral polymerases and abolish DNA synthesis. In contrast, common antibacterial drugs are rarely related to such compounds. Our work provides structural evidence that 3′-azido-substituted dTMP may serve as a potential lead for new anti-mycobacterial drugs targeting thymidylate kinase. A specific inhibition mechanism by AZTMP is revealed, which radically differs from the (pro-drug) activation mechanisms observed in the human (*24*, *25*), yeast (*26*), or *E. coli* (*16*) enzymes. AZTMP inhibits $TMPK_{Mtub}$ by excluding a Mg^{2+} ion, normally binding to the dTMP active site. We propose the following inhibition mechanism, sketched in Figure 6. Transient binding of magnesium to $TMPK_{Mtub}$ has been suggested to be promoted by partial LID closure initially prompted by a crucial water-mediated interaction between the 3′-OH group of dTMP and Asp163 (*6*). In the presence of AZTMP, the mediating Wat141 is prevented from binding. The interaction with Asp163 may therefore not take place, and the LID may not properly close. Without an appropriate steric and nucleophilic environment, normally provided by LID closure (in particular Glu166) and by the α-phosphate group of the substrate, a Mg^{2+} ion cannot be stabilized. Under these conditions, Arg95, the only positively charged residue interacting with the acceptor phosphate, is insufficient to neutralize electrostatic repulsion between the two anionic substrates. In addition, in the presence of AZTMP, the conserved P-loop residue Asp9 interacts with the azido group and is locked in a catalytically incompetent position. This further strengthens the inhibitory effect of AZTMP.

The mechanism of inhibition by AZTMP probably results from the inversion of the hydrogen bond capability of the 3′-azido substituent in this molecule versus the 3′-OH group in dTMP. A hydrogen bond donor at the 3′-position promotes stabilization of Wat141, which itself donates H-bonds to Asp163 and to one of the phosphate oxygens, favoring LID closure, stabilization of Asp9, and Mg^{2+} coordination. In

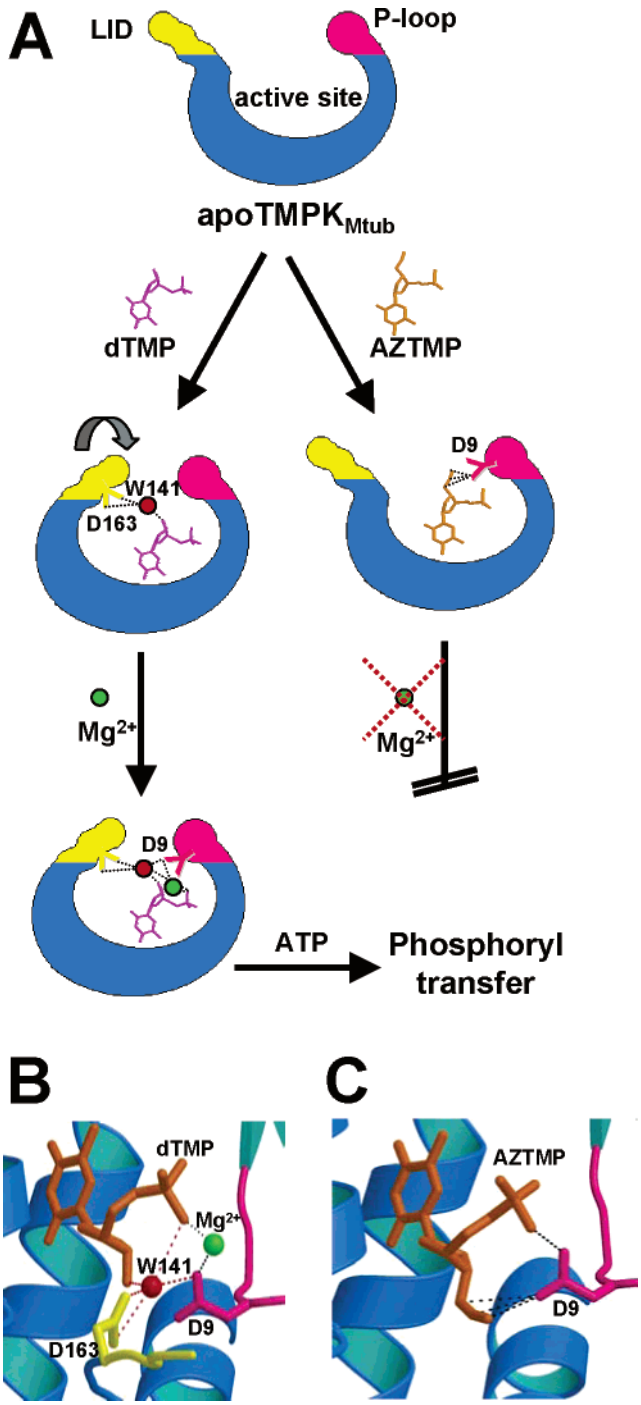

FIGURE 6: (A) Sketch of the proposed inhibition mechanism of $TMPK_{Mtub}$ by AZTMP. The normal induced-fit mechanism triggered by dTMP binding and leading to Mg^{2+} coordination and phosphoryl transfer (left) is compared with the stalling of this mechanism when AZTMP is present (right). (B) Proposed structure of the catalytically competent $TMPK_{Mtub}$−dTMP−Mg^{2+} complex (PDB entry 1N5K, monomer B). (C) Proposed structure of the inhibited $TMPK_{Mtub}$−AZTMP complex (PDB entry 1W2H, monomer A).

contrast, a hydrogen bond acceptor destabilizes this water molecule and prevents LID closure. The structure of the $TMPK_{Mtub}$−AZTMP complex in monomer A in fact closely resembles the structure of the apoenzyme (*6*), in which a major fraction of the LID as well as some extra residues at the C-terminus of the region, including Asp163 and Tyr165, are largely disordered. This suggests that the enzyme is unable to properly "sense" AZTMP, and that the induced-

fit mechanism necessary for binding Mg^{2+} and leading to catalysis may not occur in its presence.

Assessment of the nature of the interactions established by the azido group within the active site is complicated by the presence of several resonant forms of this entity, involving significant charge displacement. Nevertheless, the interaction with Asp9 probably results from long H-bonding between the carboxyl group of this residue and the N3 or N5 atom of AZTMP in a manner similar to what has been postulated in the case of binding to DNA (*27*). Such interaction, however, requires Asp9 to be protonated at the used pH. This is likely to be the case since the local electronegative environment, normally favoring Mg^{2+} binding, is expected to promote the recruitment of protons in the absence of the metal, increasing the local pK_a of Asp9. An additional interaction of an electrostatic nature between a deprotonated Asp9 and atom N4 or even N5 (*28*) carrying formal positive charges is also possible.

We propose that the "open" configuration of the phosphate acceptor site of the $TMPK_{Mtub}$−AZTMP complex, as observed in monomer A (Figure 4A,B), represents the structure of the inhibited enzyme (Figure 6C). In this open state, the 3′-azido group has only one partner, Asp9, with which to interact, and is stabilized in such a way that electron density for this group is clearly visible. In the case of monomer B, when the active site is forced to partially close due to crystal contacts (rather than due to the normal induced-fit mechanism which is arrested), the azido group interacts in a conflicting manner with several partners (Asp9, Asp163, and Tyr165), probably explaining the multiple conformations that are observed.

The inhibition of $TMPK_{Mtub}$ by thymidine, which has a 3′-OH group but no α-phosphate, also results from the impossibility of magnesium binding. However, in this case, the mechanism of magnesium exclusion has an origin different from the one described above for AZTMP. Our data suggest that $TMPK_{Mtub}$ senses thymidine correctly, as Wat141, together with Asp9, Asp163, and Tyr165, is observed in the density maps as clearly as when the natural substrate is bound. Therefore, LID closure can take place. However, a Mg^{2+} ion does not bind to the complex because in addition to LID closure, the presence of a negatively charged phosphate group is also required for metal binding. Therefore, it is not surprising that dT has also been demonstrated to be a potent inhibitor of $TMPK_{Mtub}$ (*12*).

Finally, the AZTMP molecule found in the ATP binding site of the open enzyme (Figure 5) suggests a competitive inhibition of $TMPK_{Mtub}$ by AZTMP binding to the ATP site. Such inhibition was not observed in solution studies at submillimolar concentrations of AZTMP (not shown) and is difficult to measure at the much larger concentration (14 mM) used in the crystallographic experiment because of saturation at the phosphate acceptor site. However, it has been shown to occur in yeast with a K_i of ∼30 μM (*19*). This finding is also fully consistent with the inhibition mechanism proposed for the human enzyme, where AZTMP accumulating to a millimolar level in human cells during AZT treatment would bind to the ATP site, thus contributing to the toxicity of the pro-drug (*19*).

In conclusion, our data pinpoint the need for binding a Mg^{2+} ion during catalysis as the "Achilles' heel" of *M. tuberculosis* thymidylate kinase. 3′-OH dTMP substituents which are not H-bond donors, such as AZTMP, can prevent the formation of a net of interactions linking a central water molecule (Wat141), the phosphate acceptor, the LID region, the P-loop, and in turn the metal ion, causing the induced-fit mechanism employed by the enzyme to stall.

Although a protective effect of AZT therapy against TB has been suggested in an epidemiological study (*29*), no bactericidal activity of AZT against *M. tuberculosis* cells has been detected *in vitro* (*30*). Whether AZT may penetrate the lipid-rich mycobacterial cell wall despite the presence of porin channels (*31*, *32*) remains to be assessed. Even if AZT could enter mycobacteria, AZTMP would not form due to the lack of a deoxythymidine kinase (*33*). However, since the affinities of several dT analogues for $TMPK_{Mtub}$ are similar to those of their phosphorylated congeners (*12*, *13*), AZT derivatives, possibly modified at the 5′-position, may be rationally designed on the basis of our results to inhibit the enzyme and act as potent anti-tuberculosis agents.

ACKNOWLEDGMENT

We thank Marc Delarue for many scientific discussions.

REFERENCES

1. Stokstad, E. (2000) Infectious disease. Drug-resistant TB on the rise, *Science 287*, 2391.
2. Cole, S. T. (1994) *Mycobacterium tuberculosis*: Drug-resistance mechanisms, *Trends Microbiol. 2*, 411−415.
3. Schulz, G. E. (1992) Binding of nucleotides by proteins, *Curr. Opin. Struct. Biol. 2*, 61−67.
4. Saraste, M., Sibbald, P. R., and Wittinghofer, A. (1990) The P-loop: A common motif in ATP- and GTP-binding proteins, *Trends Biochem. Sci. 15*, 430−434.
5. Li de la Sierra, I., Munier-Lehmann, H., Gilles, A. M., Barzu, O., and Delarue, M. (2001) X-ray structure of TMP kinase from *Mycobacterium tuberculosis* complexed with TMP at 1.95 Å resolution, *J. Mol. Biol. 311*, 87−100.
6. Fioravanti, E., Haouz, A., Ursby, T., Munier-Lehmann, H., Delarue, M., and Bourgeois, D. (2003) *Mycobacterium tuberculosis* thymidylate kinase: Structural studies of intermediates along the reaction pathway, *J. Mol. Biol. 327*, 1077−1092.
7. Ursby, T., Weik, M., Fioravanti, E., Delarue, M., Goeldner, M., and Bourgeois, D. (2002) Cryophotolysis of caged compounds: A technique for trapping intermediate states in protein crystals, *Acta Crystallogr. D58*, 607−614.
8. Haouz, A., Vanheusden, V., Munier-Lehmann, H., Froeyen, M., Herdewijn, P., Van Calenbergh, S., and Delarue, M. (2003) Enzymatic and structural analysis of inhibitors designed against *Mycobacterium tuberculosis* thymidylate kinase. New insights into the phosphoryl transfer mechanism, *J. Biol. Chem. 278*, 4963−4971.
9. Munier-Lehmann, H., Chaffotte, A., Pochet, S., and Labesse, G. (2001) Thymidylate kinase of *Mycobacterium tuberculosis*: A chimera sharing properties common to eukaryotic and bacterial enzymes, *Protein Sci. 10*, 1195−1205.
10. Vanheusden, V., Munier-Lehmann, H., Pochet, S., Herdewijn, P., and Van Calenbergh, S. (2002) Synthesis and evaluation of thymidine-5′-O-monophosphate analogues as inhibitors of *Mycobacterium tuberculosis* thymidylate kinase, *Bioorg. Med. Chem. Lett. 12*, 2695−2698.
11. Vanheusden, V., Munier-Lehmann, H., Froeyen, M., Dugue, L., Heyerick, A., De Keukeleire, D., Pochet, S., Busson, R., Herdewijn, P., and Van Calenbergh, S. (2003) 3′-C-Branched-chain-substituted nucleosides and nucleotides as potent inhibitors of *Mycobacterium tuberculosis* thymidine monophosphate kinase, *J. Med. Chem. 46*, 3811−3821.
12. Pochet, S., Dugue, L., Douget, D., Labesse, G., and Munier-Lehmann, H. (2002) Nucleoside Analogues as Inhibitors of Thymidylate Kinase: Possible Therapeutic Applications, *ChemBioChem 1*, 108−110.
13. Vanheusden, V., Van Rompaey, P., Munier-Lehmann, H., Pochet, S., Herdewijn, P., and Van Calenbergh, S. (2003) Thymidine and

thymidine-5′-O-monophosphate analogues as inhibitors of *Mycobacterium tuberculosis* thymidylate kinase, *Bioorg. Med. Chem. Lett. 13*, 3045−3048.
14. Pochet, S., Dugue, L., Labesse, G., Delepierre, M., and Munier-Lehmann, H. (2003) Comparative study of purine and pyrimidine nucleoside analogues acting on the thymidylate kinases of *Mycobacterium tuberculosis* and of humans, *ChemBioChem 4*, 742−747.
15. Brundiers, R., Lavie, A., Veit, T., Reinstein, J., Schlichting, I., Ostermann, N., Goody, R. S., and Konrad, M. (1999) Modifying human thymidylate kinase to potentiate azidothymidine activation, *J. Biol. Chem. 274*, 35289−35292.
16. Lavie, A., Ostermann, N., Brundiers, R., Goody, R. S., Reinstein, J., Konrad, M., and Schlichting, I. (1998) Structural basis for efficient phosphorylation of 3′-azidothymidine monophosphate by *Escherichia coli* thymidylate kinase, *Proc. Natl. Acad. Sci. U.S.A. 95*, 14045−14050.
17. Chenal-Francisque, V., Tourneux, L., Carniel, E., Christova, P., Li de la Sierra, I., Barzu, O., and Gilles, A. M. (1999) The highly similar TMP kinases of *Yersinia pestis* and *Escherichia coli* differ markedly in their AZTMP phosphorylating activity, *Eur. J. Biochem. 265*, 112−119.
18. Petit, C. M., and Koretke, K. K. (2002) Characterization of *Streptococcus pneumoniae* thymidylate kinase: Steady-state kinetics of the forward reaction and isothermal titration calorimetry, *Biochem. J. 363*, 825−831.
19. Lavie, A., Schlichting, I., Vetter, I. R., Konrad, M., Reinstein, J., and Goody, R. S. (1997) The bottleneck in AZT activation, *Nat. Med. 3*, 922−924.
20. Powell, H. R. (1999) The Rossmann Fourier autoindexing algorithm in MOSFLM, *Acta Crystallogr. D55* (Part 10), 1690−1695.
21. Brunger, A. T., Adams, P. D., Clore, G. M., DeLano, W. L., Gros, P., Grosse-Kunstleve, R. W., Jiang, J. S., Kuszewski, J., Nilges, M., Pannu, N. S., Read, R. J., Rice, L. M., Simonson, T., and Warren, G. L. (1998) Crystallography & NMR system: A new software suite for macromolecular structure determination, *Acta Crystallogr. D54* (Part 5), 905−921.
22. Jones, T. A., Zou, J. Y., Cowan, S. W., and Kjeldgaard, M. (1991) Improved methods for the building of protein models in electron density maps and the location of errors in these models, *Acta Crystallogr. A47*, 110−119.
23. De Clercq, E. (2001) Antiviral drugs: Current state of the art, *J. Clin. Virol. 22*, 73−89.
24. Ostermann, N., Lavie, A., Padiyar, S., Brundiers, R., Veit, T., Reinstein, J., Goody, R. S., Konrad, M., and Schlichting, I. (2000) Potentiating AZT activation: Structures of wild-type and mutant human thymidylate kinase suggest reasons for the mutants' improved kinetics with the HIV prodrug metabolite AZTMP, *J. Mol. Biol. 304*, 43−53.
25. Ostermann, N., Segura-Pena, D., Meier, C., Veit, T., Monnerjahn, C., Konrad, M., and Lavie, A. (2003) Structures of human thymidylate kinase in complex with prodrugs: Implications for the structure-based design of novel compounds, *Biochemistry 42*, 2568−2577.
26. Lavie, A., Vetter, I. R., Konrad, M., Goody, R. S., Reinstein, J., and Schlichting, I. (1997) Structure of thymidylate kinase reveals the cause behind the limiting step in AZT activation, *Nat. Struct. Biol. 4*, 601−604.
27. Camerman, A., Mastropaolo, D., and Camerman, N. (1987) Azidothymidine: Crystal structure and possible functional role of the azido group, *Proc. Natl. Acad. Sci. U.S.A. 84*, 8239−8242.
28. Giambasu, M. G., Diaconu, C. C., and Hillebrand, M. (2004) Electronic Structure of Some Antiviral Compounds, *Internet Electron. J. Mol. Des. 3*, 73−82.
29. McKean, L. R. (1993) Opportunistic Infections & Other Complications: Tuberculosis, *Seattle Treatment Education Project Perspective*, Vol. 5, Seattle Treatment Education Project, Seattle.
30. Elwell, L. P., Ferone, R., Freeman, G. A., Fyfe, J. A., Hill, J. A., Ray, P. H., Richards, C. A., Singer, S. C., Knick, V. B., Rideout, J. L., and Zimmerman, T. P. (1987) Antibacterial Activity and Mechanism of Action of 3′Azido-3′-Deoxythymidine (BW A509U), *Antimicrob. Agents Chemother. 31*, 274−280.
31. Faller, M., Niederweis, M., and Schulz, G. E. (2004) The structure of a mycobacterial outer-membrane channel, *Science 303*, 1189−1192.
32. Lambert, P. A. (2002) Cellular impermeability and uptake of biocides and antibiotics in Gram-positive bacteria and mycobacteria, *J. Appl. Microbiol. 92* (Suppl.), 46S−54S.
33. Saito, H., and Tomioka, H. (1984) Thymidine kinase of bacteria: Activity of the enzyme in actinomycetes and related organisms, *J. Gen. Microbiol. 130* (Part 7), 1863−1870.
34. Laskowski, R. A., MacArthur, M. W., Moss, D. S., and Thornton, J. M. (1993) PROCHECK: A program to check the stereochemical quality of protein structures, *J. Appl. Crystallogr. 26*, 283−291.
35. Esnouf, R. M. (1999) Further additions to MolScript version 1.4, including reading and contouring of electron-density maps, *Acta Crystallogr. D55* (Part 4), 938−940.
36. Merritt, E. A., and Bacon, D. J. (1997) Raster3D: Photorealistic Molecular Graphics, *Methods Enzymol. 277*, 505−524.

BI0484163